ISSN 0023-1584, Kinetics and Catalysis, 2012, Vol. 53, No. 3, pp. 409–418. © Pleiades Publishing, Ltd., 2012.
Original Russian Text © A.A. Shutilov, G.A. Zenkovets, S.V. Tsybulya, V.Yu. Gavrilov, G.N. Kryukova, 2012, published in Kinetika i Kataliz, 2012, Vol. 53, No. 3, pp. 424–434.

# Effect of the Microstructure of the Supported Catalysts $CuO/TiO_2$ and $CuO/(CeO_2–TiO_2)$ on Their Catalytic Properties in Carbon Monoxide Oxidation

**A. A. Shutilov[a, b], G. A. Zenkovets[a, b], S. V. Tsybulya[a, b], V. Yu. Gavrilov[a], and G. N. Kryukova[a]**

[a] *Boreskov Institute of Catalysis, Siberian Branch, Russian Academy of Sciences, Novosibirsk, 630090 Russia*

[b] *Novosibirsk State University, Novosibirsk, 630090 Russia*

*e-mail: alshut@catalysis.ru*

Received September 20, 2011

**Abstract**—The effect of the microstructure of titanium dioxide on the structure, thermal stability, and catalytic properties of supported $CuO/TiO_2$ and $CuO/(CeO_2–TiO_2)$ catalysts in CO oxidation was studied. The formation of a nanocrystalline structure was found in the $CuO/TiO_2$ catalysts calcined at 500°C. This nanocrystalline structure consisted of aggregated fine anatase particles about 10 nm in size and interblock boundaries between them, in which $Cu^{2+}$ ions were stabilized. Heat treatment of this catalyst at 700°C led to a change in its microstructure with the formation of fine CuO particles 2.5–3 nm in size, which were strongly bound to the surface of $TiO_2$ (anatase) with a regular well-ordered crystal structure. In the $CuO/(CeO_2–TiO_2)$ catalysts, the nanocrystalline structure of anatase was thermally more stable than in the $CuO/TiO_2$ catalyst, and it persisted up to 700°C. The study of the catalytic properties of the resulting catalysts showed that the $CuO/(CeO_2–TiO_2)$ catalysts with the nanocrystalline structure of anatase were characterized by the highest activity in CO oxidation to $CO_2$.

**DOI:** 10.1134/S0023158412030111

## INTRODUCTION

The $CuO/TiO_2$ catalysts are characterized by high activity in the selective catalytic reduction of $NO_x$ to $N_2$ with ammonia [1–7], the oxidation of CO and hydrocarbons [8–13], and also the photocatalytic oxidation of a number of harmful organic substances in air and water [14–16]. The $CuO/TiO_2$ catalysts are very promising because they are less expensive than the catalysts containing noble metals, which are in wide current use in the above processes. Because of this, the development of new methods for synthesis and the characterization of the state of the active component of the $CuO/TiO_2$ catalysts is of great scientific interest.

A considerable number of publications have been devoted to the study of the physicochemical and catalytic properties of supported $CuO/TiO_2$ catalysts. It was found that the small particle size and concentration of supported copper are the key factors responsible for high catalytic activity [1–11, 17–19]. The formation of isolated $Cu^{2+}$ and $Cu^{1+}$ ions, two-dimensional CuO clusters [1–9, 18–19], CuO clusters having chain structures [17], and copper oxide particles of different sizes [1–7, 17, 18] was detected in the $CuO/TiO_2$ catalysts, depending on the copper content and preparation method. It is believed that the fine forms of copper on the surface of $TiO_2$ in the anatase modification are stabilized by their chemical interaction. It was demonstrated [3–5, 8, 20] that the highest catalytic activity of the $CuO/TiO_2$ catalysts in CO oxidation was achieved when the surface of $TiO_2$ is coated with a monolayer of copper ion clusters.

It was found [8, 12, 13, 18, 21] that the procedure used for the preparation of copper–titanium oxide catalysts has a significant effect on the state of copper. According to Boccuzzi et al. [18], the highest degree of dispersion of copper was reached in the $CuO/TiO_2$ catalysts upon supporting copper from copper ammine solutions by adsorption followed by the hydrolysis of the adsorbed compounds, as compared to the same catalysts catalysts prepared by the traditional incipient wetness impregnation of titanium dioxide with solutions of copper salts. Tsodikov and coauthors [12, 13] prepared copper–titanium oxide catalysts with different ratios between copper and titanium by mixing the organometallic compounds of titanium and copper followed by evaporation and thermal treatment in air; these catalysts exhibited high activity CO oxidation to $CO_2$.

The main disadvantage of the $CuO/TiO_2$ catalysts is their low thermal stability. Guo et al. [10] found that the $CuO/TiO_2$ catalysts calcined at 200–350°C exhibit the highest activity in CO oxidation, and an increase in the catalyst calcination temperature led to a consid-

erable decrease in the activity. At the same time, $CuO/TiO_2$ catalysts calcined at 450–500°C have been mainly described in the literature. A decrease in the activity of the $CuO/TiO_2$ catalysts with increase of calcination temperature is due to the agglomeration of the oxide clusters of copper on the surface of anatase with the formation of large particles of the CuO phase; in turn, this accelerates the phase transition of anatase into rutile to result in a further loss of activity.

It is possible to assume that the thermal stability of copper oxide clusters in the $CuO/TiO_2$ catalysts changes upon modification of $TiO_2$ with different chemical elements. For example, Larsson and Andersson [8] found that an increase in the activity and thermal stability of the catalysts in CO oxidation was observed upon supporting copper onto titanium dioxide preliminarily modified with cerium oxide. Boccuzzi et al. [22] observed changes in the state of copper and catalytic activity in CO oxidation upon the modification of titanium dioxide with silicon oxide. Previously [23–25], we studied changes in the microstructure of anatase upon its modification with cerium, yttrium, and silicon oxides. These supports seem very promising for preparation of thermally stable copper–titanium catalysts.

In this work, we studied the effect of the microstructure of titanium dioxide on the structure, thermal stability, and catalytic properties of supported $CuO/TiO_2$ and $CuO/(CeO_2–TiO_2)$ catalysts in CO oxidation to $CO_2$.

## EXPERIMENTAL

Pure $TiO_2$ and $TiO_2$ modified with a 5–10 wt % cerium oxide were used for the preparation of the 5–7 wt % $CuO/TiO_2$ and 5–10 wt % $CuO/(CeO_2–TiO_2)$ supported catalysts. The supports—pure $TiO_2$ and $TiO_2$ containing 5–10 wt % $CeO_2$ and 90–95 wt % $TiO_2$—were prepared in accordance with a published procedure [23]. The catalysts were prepared by the incipient wetness impregnation of a support with a solution of copper nitrate followed by drying at 110°C and calcination in air at a temperature of 350–700°C for 4 h in a muffle furnace.

The electron microscopic studies were performed on a JEM 2010 instrument (JEOL, Japan) with a resolution of 1.4 Å and an accelerating voltage of 200 kV. The elemental analysis of samples (EDX) was performed with the use of an EDAX DX-4 microanalyzer with an energy-dispersive X-ray detector (Ametek, United States). The analyzed surface area was 100–150 $nm^2$, and the element detection sensitivity was 0.1 wt %.

The X-ray diffraction analysis of the samples was performed on a URD-63 diffractometer (Freiberg, Germany) with monochromatic Cu$K_\alpha$ radiation. The size of the coherent scattering region (CSR) of anatase crystallites ($d_{CSR}$, nm) was determined from the Selyakov–Scherrer formula based on the half-width of the 2.0.0 diffraction peak [26].

The oxidation numbers of cerium, copper, titanium, and oxygen ions were studied by X-ray photoelectron spectroscopy (XPS). The spectra were measured on an ES-300 photoelectron spectrometer (KRATOS Analytical, United Kingdom) in the constant pass energy mode using primary Al$K_\alpha$ and Mg$K_\alpha$ radiation. The energy scale of the spectrometer was calibrated with the use of the Au $4f_{7/2}$ binding energy of 84.0 eV. Because the reduction of $Cu^{2+}$ ions to $Cu^{1+}$ was observed at the standard power of the X-ray radiation source (205 W), the spectrum of the $CuO/TiO_2$ catalyst was measured at a decreased power of 50 W of the X-ray source and the Cu 2*p* spectra were accumulated for 2–4 min using four fresh samples; then, the spectra were averaged. All of the Cu 2*p* spectra were obtained before the onset of the reduction of $Cu^{2+}$. Spectral regions for other elements were measured after recording Cu 2*p*. Published data [27] were used in the mathematical processing of the spectra.

The specific surface area of samples ($S_{sp}$) was measured on a SORBI-M instrument (META, Russia) using the thermal desorption of argon based on four sorption equilibrium points. The pore structure of the samples was investigated by the low-temperature (77 K) sorption of nitrogen on a DigiSorb-2600 instrument (Micrometrics, the United States). The samples were preliminarily conditioned in a vacuum of $10^{-4}$ Torr at 200°C for 5 h. The mesopore size distribution was calculated from the desorption branch of the isotherm of nitrogen sorption using the classical continual Barrett–Joyner–Halenda (BJH) method [28].

The catalytic properties of the prepared catalysts were tested in CO oxidation in a flow reactor at the following composition of the reaction mixture: 0.05% CO, 5% $H_2O$, 6.7% air, and the balance nitrogen. The space velocity was 180000 $h^{-1}$, and the rate of heating was 10 K/min. The compositions of the initial and resulting reaction mixtures were determined by chromatography. Catalyst activity was characterized by the temperature at which 50% CO conversion was achieved, as determined from the curve of the temperature dependence of conversion.

## RESULTS AND DISCUSSION

Table 1 summarizes the phase compositions of the heat-treated $CuO/TiO_2$ catalysts. It is evident that only the anatase phase was detected in the $CuO/TiO_2$ catalysts containing 5–7 wt % CuO at calcination temperatures of 350–700°C. In the catalyst containing 10 wt % CuO, the appearance of traces of the copper oxide phase was detected along with anatase upon calcination at 700°C. In all of the catalysts, the size of anatase CSR ($d_{CSR}$) increased from 5 to 40–45 nm with increasing calcination temperature.

Table 2 summarizes X-ray diffraction analysis data for the $CuO/(CeO_2–TiO_2)$ catalysts calcined at 500–

**Table 1.** Effect of calcination temperature on the phase composition of the $CuO/TiO_2$ catalysts

| Catalyst composition, wt % | $T$, °C | Phase composition | $d_{CSR}$, nm |
|---|---|---|---|
| 5% CuO–95% $TiO_2$ | 350 | anatase | 5 |
| | 500 | " | 10 |
| | 700 | " | 40 |
| 7% CuO–93% $TiO_2$ | 350 | " | 6 |
| | 500 | " | 10 |
| | 700 | " | 45 |
| 10% CuO–90% $TiO_2$ | 350 | " | 6 |
| | 500 | " | 11 |
| | 700 | anatase + CuO traces | 45 |

700°C. It is evident that the phase composition of these catalysts is determined by the concentrations of copper and cerium oxides in them. Only anatase was detected in the catalyst containing 5 wt % CuO supported on a sample containing 5 wt % $CeO_2$–95 wt % $TiO_2$ after calcination in a temperature range of 500–700°C. As the copper oxide content was increased to 10 wt %, only the anatase phase was detected upon calcination at 500°C, whereas traces of the CuO phase were observed along with anatase as the temperature was increased to 700°C. At the same time, anatase and $CeO_2$ traces were detected in the 5 wt % CuO/(10 wt % $CeO_2$–90 wt % $TiO_2$) catalyst after calcination at 700°C. Phases other than anatase were not observed in the catalyst containing 10 wt % CuO prepared on the same support and calcined at 500°C. An increase in the calcination temperature to 700°C caused the appearance of $CeO_2$ and CuO traces. As in the case of the $CuO/TiO_2$ catalysts, an increase in the calcination temperature led to an increase in the $d_{CSR}$ of anatase from 10–12 to 30–40 nm in the $CuO/(CeO_2–TiO_2)$ catalysts. Note that no changes in the unit cell parameters of anatase were observed in all samples regardless concentrations of copper oxide and cerium oxide.

From electron microscopic data, it follows that the modification of titanium dioxide with copper oxide considerably changed its microstructure. Figure 1 shows an electron microscopic image of the initial titanium dioxide, which had a well-ordered regular crystal structure after calcination at 500°C. At the same time, the microstructure of titanium dioxide modified with copper oxide (Fig. 2a) after calcination at 500°C is nanocrystalline, and it consists of coalesced anatase particles (~10 nm) with a well-crystallized internal structure joined into aggregates of size 40–50 nm. This is consistent with the X-ray diffraction data, which indicate that $d_{CSR}$ = 10–11 nm. In Fig. 2, it can be seen that the microdiffraction pattern is annular, reflecting the polycrystalline nature of the aggregates, and it has somewhat broadened reflections due to the small particle size. The set of interplanar spacings corresponds to the structure of titanium dioxide in the anatase modification (marked with A in Fig. 2). Reflections from other phases were absent from the electron diffraction pattern. The high-resolution electron micrograph did not exhibit particles of other morphological forms or amorphous phases. At the same time, microanalysis data showed the presence of copper, which was uniformly distributed over the sample, in the aggregate of oxide particles (Fig. 2b). It is likely that copper is evenly located in the regions between anatase particles and, possibly, the surface of titanium oxide, without forming an individual phase or large clusters. Note that this microstructure type in the samples of $CuO/TiO_2$ calcined at 500°C was detected at a copper oxide contents of up to 10 wt %.

As the calcination temperature of the $CuO/TiO_2$ catalysts containing 5–10 wt % CuO was increased to 700°C, the particle size of anatase increased to 50 nm (Fig. 3), which is consistent with the $d_{CSR}$ data for anatase. In this case, the internal structure of anatase crystallites was regular and well-crystallized; this was reflected in the electron diffraction pattern—the

**Table 2.** Effect of calcination temperature on the phase composition of $CuO/(CeO_2–TiO_2)$ catalysts

| Catalyst composition, wt % | $T$, °C | Phase composition | $d_{CSR}$, nm |
|---|---|---|---|
| 5% CuO/(5%$CeO_2$–95%$TiO_2$) | 500 | anatase | 10 |
| 5% CuO/(5%$CeO_2$–95%$TiO_2$) | 700 | " | 30 |
| 10% CuO/(5%$CeO_2$–95%$TiO_2$) | 500 | " | 12 |
| 10% CuO/(5%$CeO_2$–95%$TiO_2$) | 700 | anatase + CuO traces | 40 |
| 5% CuO/(10%$CeO_2$–90%$TiO_2$) | 500 | anatase | 9 |
| 5% CuO/(10%$CeO_2$–90%$TiO_2$) | 700 | anatase + $CeO_2$ traces | 40 |
| 10% CuO/(10%$CeO_2$–90%$TiO_2$) | 500 | anatase | 10 |
| 10% CuO/(10%$CeO_2$–90%$TiO_2$) | 700 | anatase + $CeO_2$ traces + CuO traces | 45 |

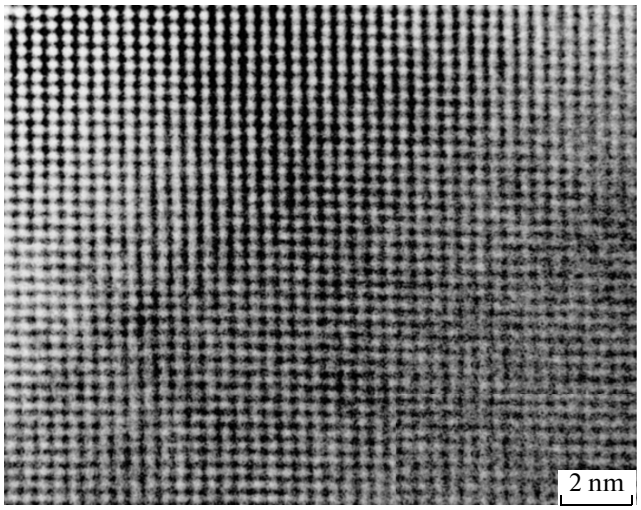


**Fig. 1.** Electron micrograph of pure $TiO_2$ calcined at 500°C.

reflections of this phase had a point character, which suggests an increase in the size of the anatase particles. These reflections are designated by A in the electron diffraction pattern given in the inset in Fig. 3, and additional weak reflections (designated by T) correspond to the CuO phase (tenorite). The values of interplanar spacing calculated for the given weak reflections correspond to the CuO phase ($d_{002} = 0.35$ and $d_{111} = 0.23$ nm). According to JCPDS data, these reflections are the most intense reflections in the structure of the CuO standard. Their low intensity is due to the fact that the particles of CuO are fine (with sizes of no greater than 2.5 nm (Fig. 3)). The particles of copper oxide sufficiently evenly covered the surface of anatase crystallites; it is likely that they were strongly bound to them because they exhibited good thermal stability at such a high temperature.

Figure 4 shows the electron micrograph of the catalyst containing 5 wt % CuO/(5 wt % $CeO_2$–95 wt % $TiO_2$) calcined at 500°C. It can be seen that its structure consisted of fine anatase crystallites with a size of 10–12 nm randomly coalesced with each other with the formation of interblock boundaries between them. In this case, the presence of any other amorphous or crystalline phases was not detected. Previously, we established that the stabilizations of cerium ions does not occur in the crystal lattice of anatase [23], and the interaction of cerium and titanium oxides occurs in an oxidizing atmosphere only at a temperature higher than 1300°C [29, 30]. In this case, changes in the unit cell parameters of anatase in comparison with standard values were also not observed. Therefore, it is possible to assume that, in the nanocrystalline structure of titanium dioxide modified with cerium oxide, cerium ions are stabilized in the region of interblock boundaries formed by coalesced anatase particles, where the structure is strongly disordered. The EDX data suggest the presence of copper in the sample; however, the occurrence of CuO particles on the surface was not observed. It is likely that copper was stabilized in the region of interblock boundaries and, partially, on the support surface without forming large clusters.

The calcination of this sample at a temperature of 700°C leads to the coarsening of anatase crystallites

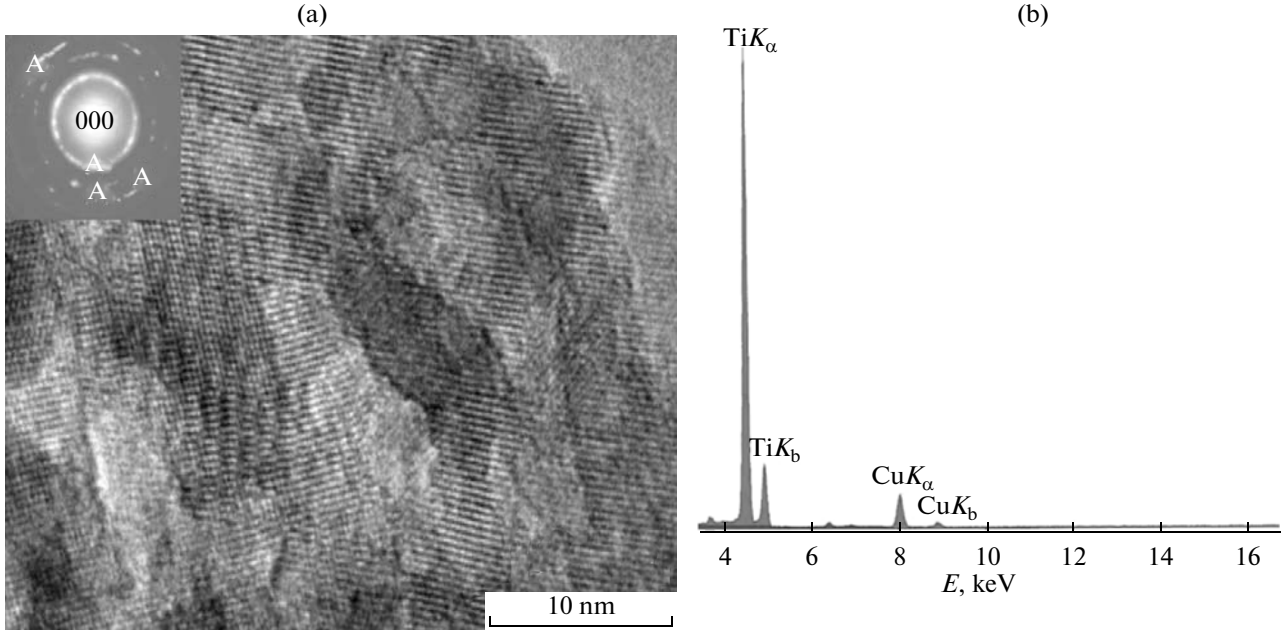


**Fig. 2.** (a) Electron micrograph of the 5 wt % $CuO/TiO_2$ catalyst calcined at 500°C and (b) the EDX spectrum of this sample.

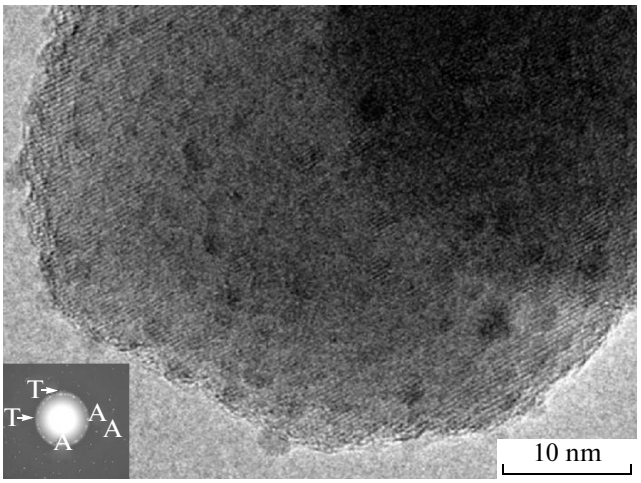


**Fig. 3.** Electron micrograph of the 5 wt % $CuO/TiO_2$ catalyst calcined at 700°C.

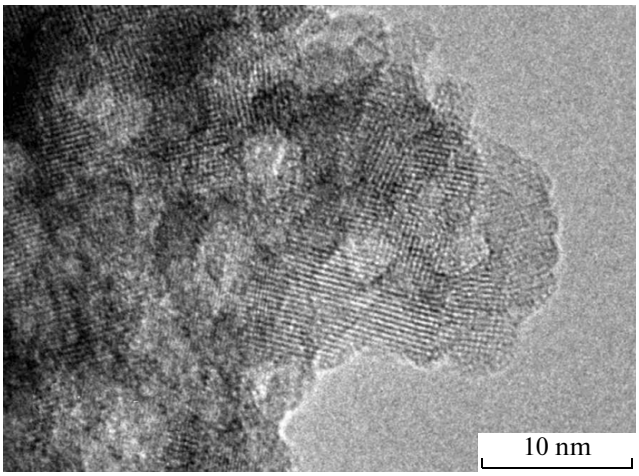


**Fig. 4.** Electron micrograph of the 5 wt % CuO/(5 wt % $CeO_2$–95 wt % $TiO_2$) catalyst calcined at 500°C.

from 10 to 35–40 nm and a notable increase in the thickness of interblock boundaries (Fig. 5). In Fig. 5, it can be seen that the structure of anatase particles in a surface layer was somewhat disordered, and this was especially pronounced at the edge of the $TiO_2$ particle. However, the structure of the catalyst in general remained nanocrystalline. According to electron microscopic data, any crystalline phases other than the phase of anatase were not observed in this catalyst. It is likely that the thermal stability of the interblock boundaries, which simultaneously contained copper and cerium ions, increased, as compared with those containing only copper ions; this can be due to the formation of Cu–Ce–O compound nuclei.

Figure 6 shows the XPS spectra measured in the characteristic regions of Ti 2*p*, O 1*s*, Ce 3*d*, and Cu 2*p* for the 5 wt % CuO/(5 wt % $CeO_2$–95 wt % $TiO_2$) catalyst calcined at 500°C. An analysis showed that a peak at 458.8 eV, which is characteristic of the Ti $2p_{3/2}$ electronic state, and a peak at 464 eV for Ti $2p_{1/2}$ were detected in the Ti 2*p* spectrum (Fig. 6a). The observed spectrum corresponds to $Ti^{4+}$ ions in $TiO_2$ [31–33].

In the region of the O 1*s* spectrum (Fig. 6b), the main peak at 529.8 eV due to $O^{2-}$ in the lattice of $TiO_2$ [32, 33] and a high-energy shoulder at 531.4 eV occurred. The second component cannot be accurately attributed; it may be hypothetically related to oxygen in a mixed oxide layer, which contains (in addition to the ions of oxygen and titanium) cerium and copper ions. However, this band can also be attributed to hydroxyl groups.

The positions of the Ce 3*d* lines in the XPS spectra Ce $3d_{5/2}$ (885.8 eV) and Ce $3d_{3/2}$ (904.3 eV), the spin–orbital splitting (18.5 eV), and the presence of a pronounced shoulder in the low-energy region unambiguously indicate the presence of only one type of $Ce^{3+}$ ions (Fig. 6c). Note that only one state of cerium ions, $Ce^{3+}$, was also detected previously in the $CeO_2$–$TiO_2$ binary system by XPS [23]. Consequently, the introduction of copper does not change the electronic state of cerium and titanium ions in the $CeO_2$–$TiO_2$ support, which was prepared by the method proposed.

Upon an analysis of the Cu 2*p* spectra, only one state of copper with the Cu $2p_{3/2}$ binding energy of 932.3 eV was detected (Fig. 6d). The position of this band, which is different from the position that corresponds to $Cu^{2+}$ ions in CuO (933.6 eV), and the absence of satellites in the region of 940–947 eV indicate that this state cannot be assigned to $Cu^{2+}$ ions. It is most likely that the apparent Cu $2p_{3/2}$ binding energy can be related to the state of $Cu^{1+}$ ions because the Cu $2p_{3/2}$ binding energy is 932.5 eV for $Cu_2O$ [33]. However, the observed binding energy of the Cu $2p_{3/2}$ peak was shifted toward lower binding energies, as compared with that of bulk $Cu_2O$; this can be due to

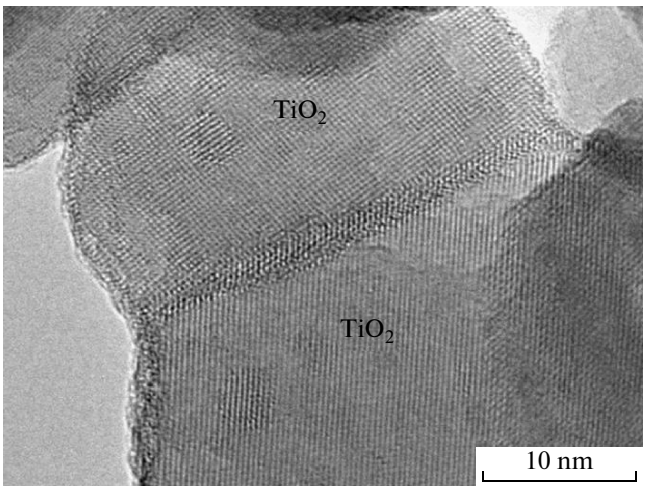


**Fig. 5.** Electron micrograph of the 5 wt % CuO/(5 wt % $CeO_2$–95 wt % $TiO_2$) catalyst calcined at 700°C.

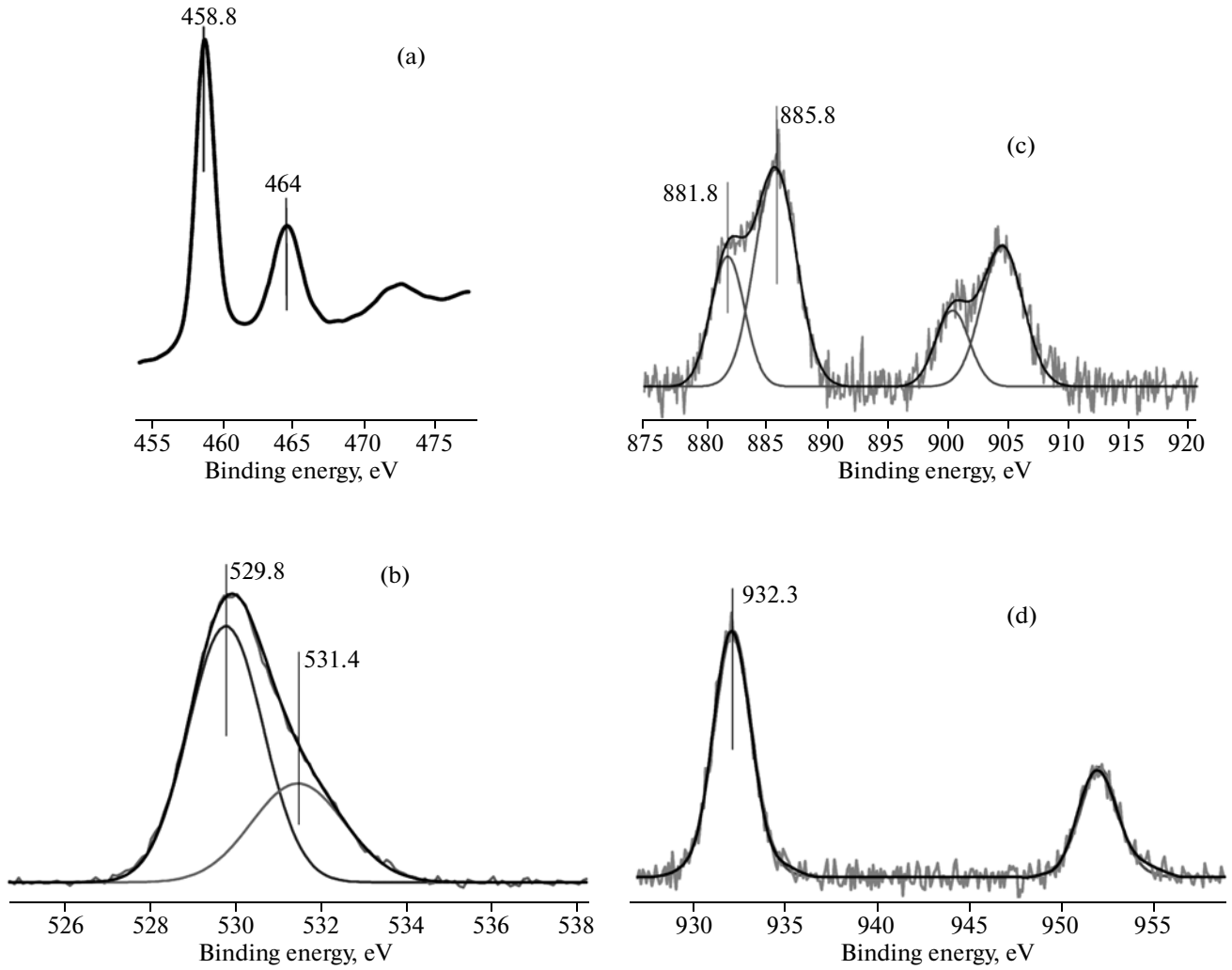


**Fig. 6.** XPS spectra of the (a) Ti 2*p*, (b) O 1*s*, (c) Ce 3*d*, and (d) Cu 2*p* regions of the 5 wt % CuO/(5 wt % $CeO_2$–95 wt % $TiO_2$) catalyst calcined at 500°C.

the high degree of dispersion of $Cu^{1+}$ ions, which strongly interact with the support [34].

The XPS spectra of the 5 wt % CuO/$TiO_2$ catalyst calcined at 500°C are shown in Fig. 7. The Ti 2*p* spectrum (as in the previous sample) exhibited a peak at 458.8 eV characteristic of the Ti $2p_{3/2}$ state and a peak at 464 eV for Ti $2p_{1/2}$ (Fig. 7a), which are due to the $Ti^{4+}$ ions in $TiO_2$. No additional lines corresponding to other titanium compounds were observed.

Several peaks can be distinguished in the O 1*s* spectrum (Fig. 7b). The most intense peak at BE = 529.9 eV belongs to oxygen in the structure of $TiO_2$, and low-intensity peaks with BE = 531.7 and 533.0 eV can be related to oxygen in a mixed oxide layer, which contained titanium and copper ions, and also to hydroxyl groups.

In the Cu 2*p* spectrum, a satellite at BE = 940–945 eV, which unambiguously suggests the presence of $Cu^{2+}$, and a peak that characterizes the Cu $2p_{3/2}$ state of copper can be recognized. The latter peak can be decomposed into the main peak at BE = 935.8 eV and an additional peak at BE = 933.9 eV, and they can be related to $Cu^{2+}$ ions [32].

The supporting of copper oxide on both titanium dioxide with no additives and titanium dioxide modified with cerium oxide affected the formation of the specific surface area and pore structure of catalysts. Table 3 summarizes the texture parameters of titanium dioxide samples modified with cerium oxide and copper oxide calcined at 500 and 700°C. From the data given in Table 3, it follows that the modification of samples with copper oxide leads to a decrease in the specific surface areas of all of the samples. Simultaneously, an increase in the copper oxide content of the samples calcined at 500 and 700°C was accompanied by a progressive decrease in the surface area. At the same time, the modification of titanium dioxide with cerium oxide facilitates the retention of a larger specific surface area and, as a rule, a larger pore volume under comparable heat treatment conditions. The

mesopore volume of the initial $TiO_2$ support containing 5 wt % $CeO_2$ at 500°C was 0.292 $cm^3/g$. In the samples calcined at 500°C, the introduction of a copper oxide additive in an amount of 1 wt % led to a decrease in the mesopore volume to 0.272 $cm^3/g$; however, the pore volume changed only slightly as the CuO content was further increased to 10 wt %. Upon the addition of 1 wt % copper oxide, the predominant pore size $d_{pr}$ increased by a factor of about 2 and remained almost unchanged as the concentration of copper oxide in the sample was increased. This fact suggests that, in this case, the mechanism of the surface-diffusion agglomeration of $TiO_2$ particles occurred. Upon thermal treatment at 700°C, the higher the copper content of copper–titanium samples, the more strongly decreased the specific surface area and mesopore volume of the samples. At the same time, the predominant pore diameter ($d_{pr}$) increased; this increase was the most significant at a CuO content of the sample of 5 wt % or higher. This suggests the sintering of samples predominantly by the bulk viscous flow mechanism.

Figures 8 and 9 show the temperature dependence of the conversion of CO for the samples. In Fig. 8, it can be seen that 50% CO conversion was reached at a reaction temperature of 206°C for the 5 wt % $CuO/TiO_2$ catalyst calcined at 500°C. After calcination at 700°C, the catalyst activity somewhat increased: the conversion of CO as high as 50% was attained at 187°C. The temperature dependence of the conversion of CO on the 7 wt % $CuO/TiO_2$ catalyst also calcined at 500 and 700°C exhibited an analogous character, although the corresponding temperatures at which the conversion of CO reached 50% were lower than those for the previous catalyst; this was due to a higher copper oxide content. Thus, the temperature at which a 50% conversion of CO was reached was 192°C for the 7 wt % $CuO/TiO_2$ catalyst calcined at 500°C, and it decreased to 172°C after the calcination of the catalyst at 700°C. The difference in the catalytic properties of the $CuO/TiO_2$ catalysts calcined at 500 and 700°C can be caused by different states of copper in these catalysts.

Upon the supporting of copper oxide on titanium dioxide modified with cerium oxide, the activity of the $CuO/(CeO_2–TiO_2)$ catalysts was higher than that of the $CuO/TiO_2$ catalysts at the same copper oxide contents (Fig. 9). For the 5 wt % CuO/(5 wt % $CeO_2$–95 wt % $TiO_2$) catalyst calcined at 500°C, a 50% conversion of CO was reached at 135°C, and then it remained unchanged after catalyst calcination at 700°C. An increase in the cerium oxide content of the support to 10 wt % with the retention of a copper oxide content of 5 wt % CuO led to an insignificant increase in the catalyst activity (the conversion of CO reached 50% at a temperature of 130°C), which, as in the previous case, remained unchanged as the catalyst calcination temperature was increased from 500 to 700°C. It is likely that an increase in the activity of these catalysts, as compared with the $CuO/TiO_2$ catalysts, can be due to the retention of the nanocrystalline structure of the catalysts in this calcination temperature range and the presence of $Cu^{1+}$ ions. As found by Larsson and Andersson [8], these ions are the most active centers, at which the reaction of CO oxidation to $CO_2$ occurs. As in two previous cases, the high catalyst activity was observed upon increasing the copper oxide content of the 10 wt % CuO/(5 wt % $CeO_2$–95 wt % $TiO_2$) catalyst after calcination at 500°C (the conversion of CO was 50% at a temperature of 127°C), whereas the activity decreased considerably after calcination at 700°C (the conversion of CO was 50% at 155°C) (Fig. 9). Based on a comparison between X-ray diffraction data and catalytic properties, we can

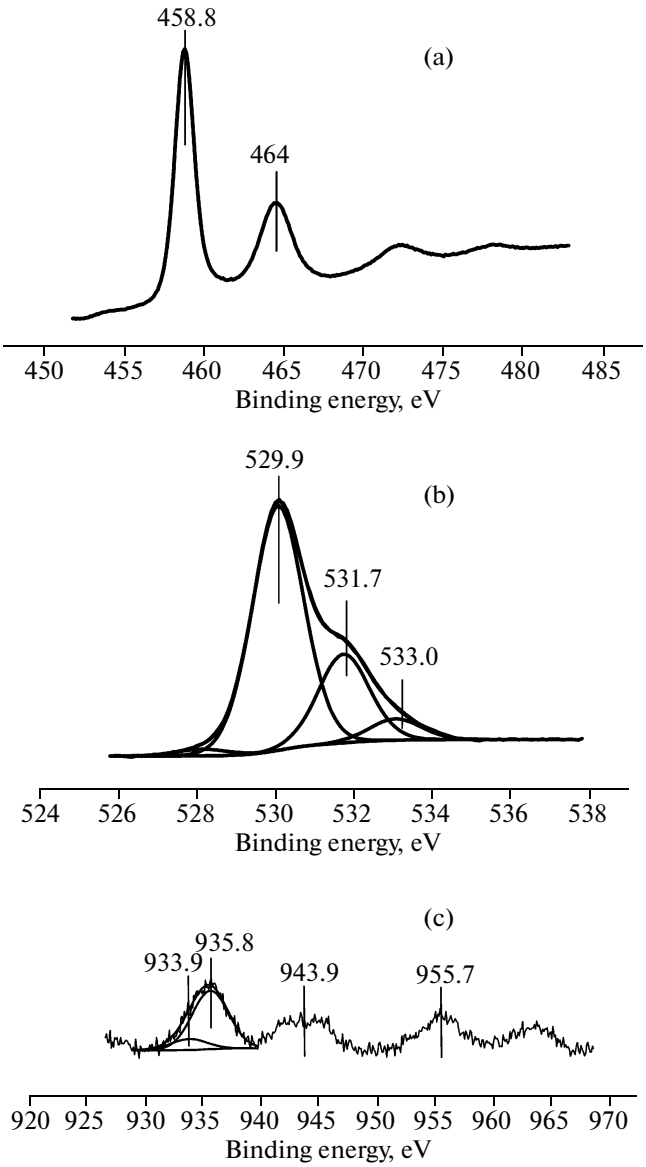


**Fig. 7.** XPS spectra of the (a) Ti 2*p*, (b) O 1*s*, and (c) Cu 2*p* regions of the 5 wt % $CuO/TiO_2$ catalyst calcined at 500°C.

**Table 3.** Effect of calcination temperature on the pore structure parameters of $CuO/TiO_2$ and $CuO/(CeO_2–TiO_2)$ catalysts

| Catalyst composition, wt % | $T$, °C | $S_{BET}$, $m^2/g$ | $V_s$, $cm^3/g$ | $d_{pr}$, nm |
|---|---|---|---|---|
| $5\%CeO_2–95\%TiO_2$ | 500 | 196 | 0.292 | 2.5 |
| $1\%\ CuO/TiO_2$ | 500 | 113 | 0.256 | 3.5 |
| $1\%\ CuO/(5\%CeO_2–95\%TiO_2)$ | 500 | 142 | 0.272 | 4.6 |
| $5\%\ CuO/TiO_2$ | 500 | 96 | 0.226 | 4.4 |
| $5\%\ CuO/(5\%CeO_2–95\%TiO_2)$ | 500 | 122 | 0.269 | 4.6 |
| $10\%\ CuO/TiO_2$ | 500 | 83 | 0.293 | 5.7 |
| $10\%\ CuO/(5\%CeO_2–95\%TiO_2)$ | 500 | 99 | 0.259 | 4.6 |
| $5\%CeO_2–95\%TiO_2$ | 700 | 55 | 0.276 | 7.5 |
| $1\%\ CuO/TiO_2$ | 700 | 25 | 0.138 | 19 |
| $1\%\ CuO/(5\%CeO_2–95\%TiO_2)$ | 700 | 43 | 0.269 | 7.1 |
| $5\%\ CuO/TiO_2$ | 700 | 12 | 0.085 | 58 |
| $5\%\ CuO/(5\%CeO_2–95\%TiO_2)$ | 700 | 20 | 0.146 | 17.6 |
| $10\%\ CuO/TiO_2$ | 700 | 8 | 0.062 | – |
| $10\%\ CuO/(5\%CeO_2–95\%TiO_2)$ | 700 | 15 | 0.134 | 29.3 |

Note: $S_{BET}$ is the specific surface area; $V_s$ is the mesopore volume; and $d_{pr}$ is the predominant mesopore diameter, as determined by the BJH method.

assume that the decrease in the activity of this catalyst after calcination at 700°C was caused by the partial destruction of the catalyst microstructure with the release of a trace coarse phase of copper oxide.

Thus, the results of this study show that the formation of a nanocrystalline anatase structure occurred upon supporting 5–10 wt % copper oxide on titanium dioxide, which consisted of fine anatase particles, after calcination at 500°C. In this structure type, $Cu^{2+}$ ions are mainly stabilized at interblock boundaries formed by coalesced anatase particles and, possibly, on the surface without forming an individual phase or large clusters. It is believed that, as the calcination temperature of the $CuO/TiO_2$ catalysts was increased to 700°C, the agglomeration of copper ions initially occurred in the region of interblock boundaries with the formation of fine copper oxide clusters. fine CuO particles with sizes of 2.5–3 nm, which were strongly bound to the surface of anatase, were subsequently formed from these clusters (at a copper oxide content of less than 10 wt %); because of this, they possess sufficiently high thermal stability at this high temperature

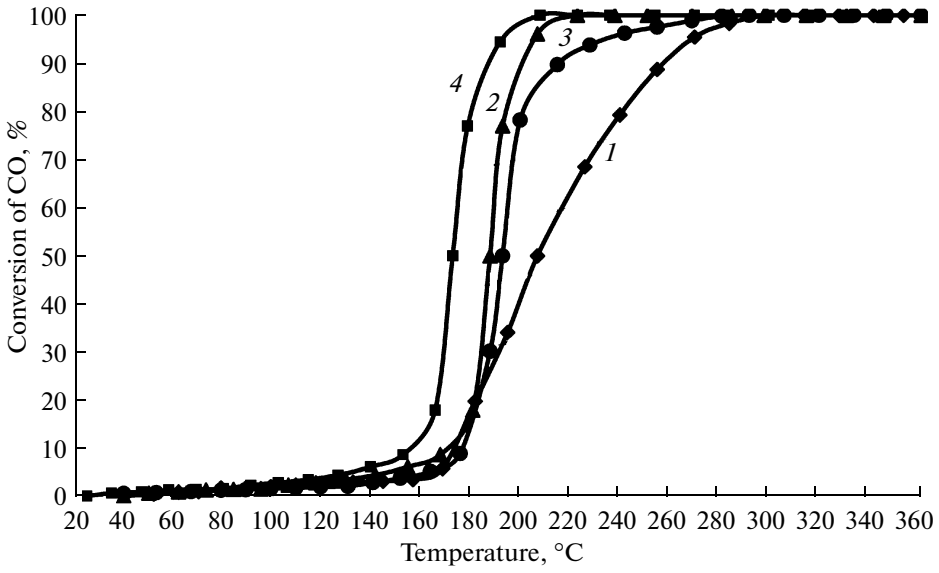


**Fig. 8.** Effect of temperature on the conversion of CO in its oxidation to $CO_2$ on the following catalysts: 5 wt % CuO/(5 wt % $CeO_2$–95 wt % $TiO_2$) calcined at (*1*) 500 or (*2*) 700°C and 7 wt % $CuO/TiO_2$ calcined at (*3*) 500 and (*4*) 700°C.

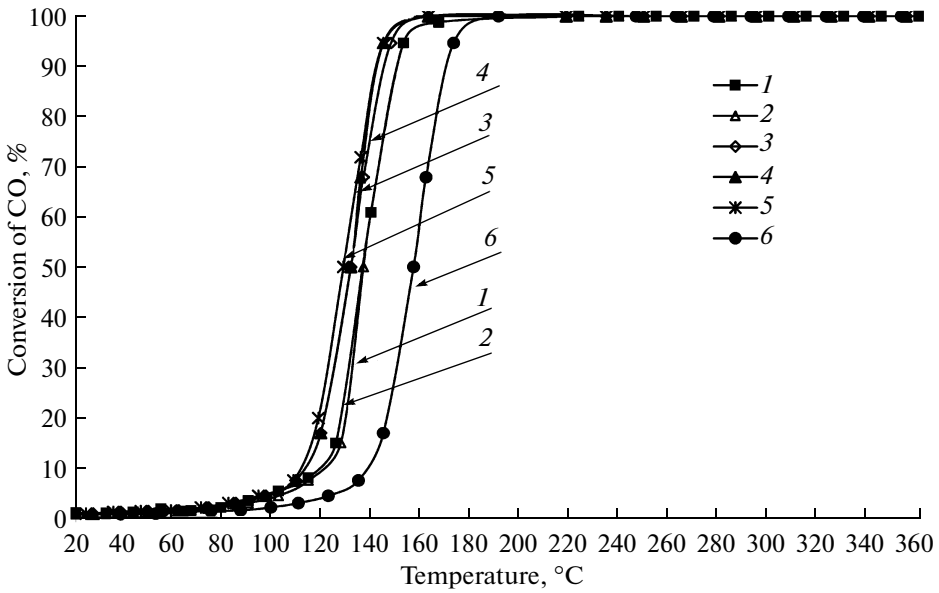


**Fig. 9.** Effect of temperature on the conversion of CO in its oxidation to $CO_2$ on the following catalysts: 5 wt % $CuO/(5$ wt % $CeO_2$–95 wt % $TiO_2)$ calcined at (*1*) 500 or (*2*) 700°C; 5 wt % $CuO/(10$ wt % $CeO_2$–90 wt % $TiO_2)$ calcined at (*3*) 500 or (*4*) 700°C; and 10 wt % $CuO/(5$ wt % $CeO_2$–95 wt % $TiO_2)$ calcined at (*5*) 500 or (*6*) 700°C.

of calcination. Upon the release of copper from the region of interblock boundaries, the destruction of a nanocrystalline structure and the formation of a well-ordered anatase structure occurred. It is interesting to note that, in this case, the particles of copper oxide stabilized on the surface of anatase are uniformly distributed over the surface. Note that, at a copper oxide content of 5–7 wt %, a coarse CuO phase was not formed on the surface of $TiO_2$, but it was detected at a higher content of 10 wt % $CuO/TiO_2$. For example, the formation of the coarse CuO phase was observed in the $CuO/TiO_2$ catalysts prepared by other methods and calcined at lower temperatures [11, 35]. Attention should also be focused on the fact that, in the test catalysts, an increase in the calcination temperature caused a decrease in the specific surface area and a change in the pore structure. However, the phase of anatase is stable upon heat treatment up to 700°C, as confirmed by X-ray diffraction analysis and electron microscopic data. At the same time, in a number of other publications, the onset of a phase transition of anatase to rutile in the $CuO/TiO_2$ catalysts in the presence of a coarse CuO phase was noted even at calcination temperatures higher than 450–500°C. The experimental data indicate that the microstructure of the $CuO/TiO_2$ catalysts has also an effect on their catalytic activity in the reaction of CO oxidation. The 5–7 wt % $CuO/TiO_2$ catalysts, which contained fine copper oxide particles stabilized on the surface of anatase with a regular crystal structure, were more active that the catalysts that have the nanocrystalline structure of anatase.

Upon the supporting of 5–10 wt % CuO on titanium dioxide modified with 5–10 wt % cerium oxide, the $CuO/(CeO_2–TiO_2)$ catalysts with the nanocrystalline structure of anatase were formed after thermal treatment at 500°C. The structure consisted of incoherently coalesced anatase crystallites with the formation of interblock boundaries between them, in which $Ce^{3+}$ and $Cu^{1+}$ ions were stabilized. Note that our previous XPS studies of the microstructure and electronic state of cerium ions in a $CeO_2–TiO_2$ support [23] showed that cerium ions stabilized in the region of interblock boundaries also had the oxidation state $Ce^{3+}$. It was assumed [8, 36] that the states $Ce^{3+}$ and $Cu^{1+}$ in the $CuO/(CeO_2–TiO_2)$ catalysts were caused by the action of X-ray photoelectron radiation because an increase in the concentrations of $Ce^{3+}$ and $Cu^{1+}$ ions with exposure time was observed. In our case, we failed to detect of the states $Ce^{4+}$ and $Cu^{2+}$ in the 5 wt % $CuO/(5$ wt % $CeO_2$–95 wt % $TiO_2)$ catalyst by XPS. The calcination of catalysts containing 5–7 wt % CuO and 5–10 wt % $CeO_2$ at a temperature of 700°C led to a considerable increase in the size of anatase crystallites from 10 to 30 nm. However, in this case, according to electron microscopic data, their microstructure remained nanocrystalline with well-marked interblock boundaries, in which the nuclei of Cu–Ce–Ti–O or Cu–Ce–O compounds can be formed. It is likely that the simultaneous presence of cerium and copper ions in the region of interblock boundaries enhances their higher thermal stability, as compared with interblock boundaries in the $CuO/TiO_2$ catalysts stabilized by only copper ions. Note that the catalysts containing 5–10 wt % $CuO/(5$–10 wt % $CeO_2$–95–90 wt % $TiO_2)$ and calcined at a temperature of 500°C were uniform in terms of phase composition and contained only an anatase phase. After calcination at 700°C,

copper oxide and cerium oxide phases were detected in addition to anatase in the catalysts containing 10 wt % CuO and 5–10 wt % $CeO_2$. This fact suggests that the concentration of cerium and copper ions that can be stabilized in the region of interblock boundaries decreased with the temperature of catalyst calcination. The studies of the catalytic activity of the catalysts containing 5–7 wt % CuO/(5–10 wt % $CeO_2$–95–90 wt % $TiO_2$) in the reaction of CO oxidation showed that the activity remained unchanged as the catalyst calcination temperature was increased from 500 to 700°C. According to electron microscopic data, this was due to the retention of the nanocrystalline structure of anatase at a high calcination temperature.

## ACKNOWLEDGMENTS

We are grateful to A.I. Boronin and I.P. Prosvirin for performing the XPS studies of the catalysts. This work was supported by the Siberian Branch of the Russian Academy of Sciences (interdisciplinary project no. 36), the Ministry of Education and Science of the Russian Federation (project no. 2.1.1/729; state contract 16.513.11.3091), and the President of the Russian Federation (grant no. MK-6688.2012.3).

## REFERENCES

1. Centi, G., Nigro, C., Perathoner, S., and Stella, G., *Catal. Today*, 1993, vol. 17, p. 159.
2. Centi, G., Perathoner, S., Kartheuser, B., Hodnett, B.K., and Stella, G., *Catal. Today*, 1993, vol. 17, p. 103.
3. Centi, G., Perathoner, S., Kartheuser, B., Rohan, D., and Hodnett, B.K., *Appl. Catal., B*, 1992, vol. 1, p. 129.
4. Centri, G. and Perathoner, S., *Appl. Catal., A*, 1995, vol. 132, p. 179.
5. Komova, O.V., Simakov, A.V., Tzykoza, L.T., Sasonova, N.N., Ushakov, A.V., Barannik, G.B., and Ismagilov, Z.R., *React. Kinet. Catal. Lett.*, 1995, vol. 54, p. 361.
6. Schoenmarker-Stolk, M.C., Verwijs, J.M., and Scholten, J.F., *Appl. Catal., A*, 1987, vol. 30, p. 339.
7. Taylor, K.C., *Catal. Rev. Sci. Eng.*, 1993, vol. 35, p. 457.
8. Larsson, P.O. and Andersson, A., *J. Catal.*, 1998, vol. 179, p. 72.
9. Larsson, P.O., Andersson, A., Wallenberg, B., and Svensson, B., *J. Catal.*, 1996, vol. 163, p. 279.
10. Guo, X.-Z., Huang, J., Wang, S.-R., Wang, Y.-M., Zang, B.-L., and Wu, S.-H., *J. Dispersion Sci. Technol.*, 2009, vol. 30, p. 1114.
11. Huang, J., Wang, Sh., Zhao, Y., Wang, X., Wang, Sh., Wu, Sh., Zhang, Sh., and Huang, W., *Catal. Commun.*, 2006, no. 7, p. 1029.
12. Tsodikov, M.V., Trusova, Ye.A., Slivinskii, Ye.V., Hernandez, G.G., Kochubey, D.I., Lipovich, V.G., and Navio, J.A., *Stud. Surf. Sci. Catal.*, 1998, vol. 127, p. 679.
13. Trusova, E.A., Tsodikov, M.V., Slivinskii, E.V., Hernandez, G.G., Bukhtenko, O.V., Zhdanova, T.N., Kochubey, D.I., and Navio, J.A., *Mendeleev Commun.*, 1998, no. 3, p. 102.
14. Chen, C.-S., You, J.-H., Lin, J.-H., and Chen, Y.Y., *Catal. Commun.*, 2008, vol. 9, p. 2381.
15. Arana, J., Rodriguez, C.F., Diaz, O.G., Melian, J.A.H., and Pena, J.P., *Catal. Today*, 2005, vol. 101, p. 261.
16. Chiang, K., Amal, R., and Tran, T., *Adv. Environ. Res.*, 2002, vol. 6, p. 471.
17. Komova, O.V., Simakov, A.V., Rogov, V.A., Kochubei, D.I., Odegova, G.V., Kriventsov, V.V., Paukshtis, E.A., Ushakov, V.A., Sasonova, N.N., and Nikoro, T.A., *J. Mol. Catal. A: Chem.*, 2000, vol. 161, nos. 1–2, p. 191.
18. Boccuzzi, F., Chiorino, A., Martra, G., Gargano, M., Ravasio, N., and Carrozzini, B., *J. Catal.*, 1997, vol. 165, no. 2, p. 129.
19. Boccuzzi, F., Chiorino, A., Martra, G., Gargano, M., Ravasio, N., and Carrozzini, B., *J. Catal.*, 1997, vol. 165, no. 2, p. 140.
20. Yu, X.-F., Wu, N.-Z., Xie, Y.-C., and Tang, Y.-Q., *J. Mater. Chem.*, 2000, vol. 10, p. 1629.
21. Zhu, H., Wu, Y., Zhao, X., Wan, H., Yang, L., Hong, J., Yu, Q., Dong, L., Chen, Y., Jian, C., Wei, J., and Xu, P., *J. Mol. Catal. A: Chem.*, 2006, vol. 243, no. 1, p. 24.
22. Boccuzzi, F., Coluccia, S., Martra, G., and Ravasio, N., *J. Catal.*, 1999, vol. 184, no. 2, p. 316.
23. Zenkovets, G.A., Shutilov, A.A., Gavrilov, V.Yu., Tsybulya, S.V., and Kryukova, G.N., *Kinet. Catal.*, 2007, vol. 48, no. 5, p. 742.
24. Shutilov, A.A., Zenkovets, G.A., Gavrilov, V.Yu., and Tsybulya, S.V., *Kinet. Catal.*, 2011, vol. 52, no. 1, p. 111.
25. Zenkovets, G.A., Gavrilov, V.Yu., Shutilov, A.A., and Tsybulya, S.V., *Kinet. Catal.*, 2009, vol. 50, no. 5, p. 760.
26. Guinier, A., *Theorie et technique de la radiocristallographie*, Paris: Dunot, 1956.
27. Sherwood, P.M.A., in *Practical Surface Analysis by Auger and X-ray Photoelectron Spectroscopy*, Briggs, D. and Seah, M.P., Eds., Chichester: Wiley, 1983, p. 555.
28. Barret, E.P., Joyner, L.G., and Hallenda, P.H., *J. Am. Chem. Soc.*, 1951, vol. 73, no. 1, p. 373.
29. Leonov, A.I., *Vysokotemperaturnaya khimiya kislorodnye soedinenii tseriya* (High-Temperature Chemistry of Oxygen-Containing Cerium Compounds), Leningrad: Nauka, 1970.
30. Leonov, A.I., Piryutko, M.M., and Keller, E.K., *Izv. Akad. Nauk SSSR*, 1966, no. 5, p. 787.
31. Sinha, A.K. and Suzuki, K., *J. Phys. Chem. B*, 2001, vol. 109, no. 5, p. 1708.
32. *Handbook of X-Ray Photoelectron Spectroscopy*, Moulder, J.F., Stickle, W.F., Sobol, P.E., et al., Eds., Eden Prairie, Minn.: PerkinElmer Corp., Physical electronics Division, 1992.
33. Wagner, C.D., Naumkin, A.V., Kraut-Vass, A., Allison, J.W., Powell, C.J., and Rumble, C.J., NIST X-Ray Photoelectron Spectroscopy Database, Version 3.5, National Institute of Standards and Technology, Gaithersburg, 2003. http://srdata.nist.gov/xps
34. Mason, M.G., *Phys. Rev.*, 1983, vol. 27, p. 748.
35. Zang, J., Li, M.-J., Feng, Z.-C., Chen, J., and Li, C., *J. Phys. Chem. B*, 2006, vol. 110, p. 927.
36. Zou, Zh.-Q., Meng, M., Guo, L.-H., and Zha, Yu.-Q., *J. Hazard. Mater.*, 2009, vol. 163, p. 835.